Electrically controlled polarization rotator using nematic liquid crystal

TENGHAO LI, QINGMING CHEN, AND XUMING ZHANG[*]

Department of Applied Physics, the Hong Kong Polytechnic University, Hung Hom, Kowloon, Hong Kong S.A.R., China
[*]*apzhang@polyu.edu.hk*

Abstract: Here we report a planar polarization rotator using a nematic liquid crystal waveguide, which is subject to a gradient electric field in parallel to the waveguide substrate plane. The fabricated polydimethylsiloxane (PDMS) device has demonstrated the electrically-controlled polarization rotation at a switching time of 70 ms and a propagation loss of 9 dB/cm at 532 nm. The unique features such as planar form, electric control, and soft material allows integration into planar lightwave circuits and flexible photonics.

1. Introduction

Electrically-switchable polarization rotation (PR) has long been the underlying mechanism for liquid crystal displays, which is induced by the twisted nematic liquid crystal (NLC) to the free-space propagating light [1]. Recently, some numerical studies have been proposed to investigate and apply the fiber/waveguide-based NLC PR [2,3]. The PR for microwave is presented in LC device [4], and the Berry phase PR is also demonstrated in the silicon chip [5]. However, no direct experiment evidence is ever reported on the corresponding effect in the planar optical waveguide form. In this paper, a flexible electrically-switchable NLC-PR is proposed and experimentally demonstrated in the optofluidic waveguide [6].

2. Principle

The principle of the NLC-PR is sketched in Fig. 1(a). The mechanism is to pre-align vertically the NLC in the waveguide, and then to apply a gradient electric field to drag the NLC gradually to the planar direction along the waveguide when polarization rotation is needed. It mimics the free-space PR using twisted nematic (TN) effect [1]. When the Mauguin condition [7] is met, the polarization rotation can be achieved.

In theory, the NLC is commonly modeled as the composite of rod-like molecule in physics, and the NLC of 5CB is uniaxial [1]. In the proposed device, the NLC orientation configuration is determined by both the surface alignment and the external electric field. According to the Oseen-Frank continuum elastic theory [1,2], it satisfies the minimization of total free energy F_{tot}, which is defined as the volume integral of free energy density F_d, as given by:

$$F_{tot} = \iiint_V f_d \, dV = \iiint_V f_{ela} + f_E \, dV, \tag{1}$$

where f_d composes of two terms in the presence of external electric field, namely the elastic free energy f_{ela} and the electric-field free energy f_E.

With the local NLC director, the local permittivity of the NLC is defined as:

$$\varepsilon = \begin{bmatrix} \varepsilon_\perp + \Delta\varepsilon n_x n_x & \Delta\varepsilon n_y n_x & \Delta\varepsilon n_z n_x \\ \Delta\varepsilon n_x n_y & \varepsilon_\perp + \Delta\varepsilon n_y n_y & \Delta\varepsilon n_z n_y \\ \Delta\varepsilon n_x n_z & \Delta\varepsilon n_y n_z & \varepsilon_\perp + \Delta\varepsilon n_z n_z \end{bmatrix}, \tag{2}$$

in which NLC molecule director $\mathbf{n} = (n_x, n_y, n_z)$, and the dielectric anisotropy $\Delta\varepsilon = \varepsilon_{//} - \varepsilon_{\perp}$ with the components $\varepsilon_{//}$ and $\varepsilon_{\perp}$. The light propagation along the NLC waveguide can be further calculated using the NLC permittivity distribution, in case that the light power is low enough to prevent the optical nonlinearity effect [8].

Based on the above mechanism and theory, a sample design is proposed as shown in Fig. 1(b) and 1(c), with the spatial coordinate O-XYZ defined for clear illustration.
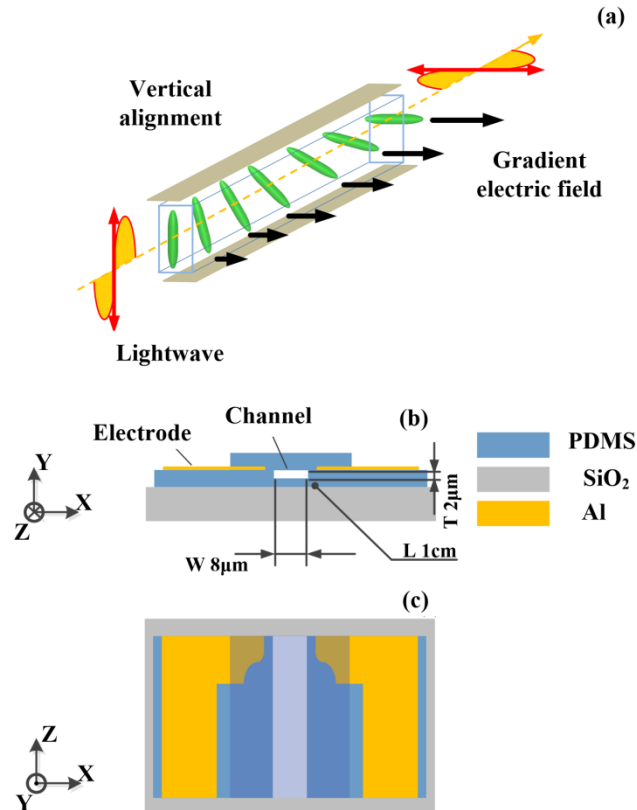

Fig. 1. Device design of the planar polarization rotator in the waveguide form. (a) Physic mechanism; (b) cross-sectional end view, and (c) top view. The spatial coordinate O-XYZ is also defined and presented in (b) and (c). The width (W), the thickness (T), and also the length (L) of the channel are about 8 μm, 2 μm and 1 cm, respectively.

The main structure of the device is a straight channel surrounded by cured polydimethylsiloxane (PDMS), and the channel is filled with the NLC (e.g. 5CB). Due to the hydrophobic property, the PDMS surface can be used directly for homeotropic alignment of NLC [6]. The cross-section of the channel is in the shape of rectangle, whose thickness is smaller than its width, with the aspect ratio of about 1:4 (see Fig. 1(b)). The alignment effect is thus more evident in the direction perpendicular to the substrate than the other one. In the design, the channel has the width of 8 μm, the thickness of 2 μm, and the total length of 1 cm, respectively.

A pair of electrodes is also placed on both sides of the channel. As shown in Fig. 1(c), the electrodes are patterned to have a gradually increased separation between them so that a driving voltage would generate a gradient electric field, which is key to the polarization rotation. Each electrode consists of a straight portion and two arcs which are tangential to each other at the junction. The bending angle of the two arcs is 0.472 rad. The bending radius of the arc adjacent to the straight waveguide is 11 μm, while the radius of the other arc is 99

μm. The outer parts are extended to ease the electrical connection in the experiments. The glass slide is used as the substrate for rigid support of device.

3. Fabrication

Different from the passive PDMS waveguide [6], the metal electrodes (aluminum here) should be fabricated for switching function. The sample fabrication process includes mainly 8 steps, as shown in the flow char in Fig. 2.

It starts from the straight channel fabrication in PDMS substrate using the molding method (Steps 1-2). The mold is prepared by patterning AZ5214 photoresist on a hard substrate (e.g., silicon wafer) using photolithography. The straight pattern is about 2 μm in thickness and 8 μm in width as characterized by the surface profiler. The PDMS mixture (Sylgard 184 Elastomer, with the vinyl-terminated base and the curing agent mixed in weight ratio of 10:1) is poured onto the mold, placed horizontally and heated at temperature of 95 °C for 2 hours. The cured and solid PDMS is then peeled off from the mold, flipped up and bonded against a glass slide using oxygen plasma treatment (power of 50 W for 30 s).

The Al electrodes are then fabricated on the PDMS film using a complicated process of later 5 steps. The key idea is to use a thin film of Al to modify the surface property of PDMS, which makes it possible to further spin-coat AZ5214 photoresist on the PDMS film.

The Al thin film (about 16 nm in thickness) is first deposited on the PDMS film by magnetron sputtering (Step 3). With the help of Al thin film, AZ5214 mask (reversed to the electrodes) is fabricated by photolithography and an additional developing step (Step 4). The Al electrodes (about 160 nm in thickness) are then deposited by magnetron sputtering (Step 5) and go through the lift-off process in acetone (Step 6). Strong adhesion of Al to PDMS is formed, making it tolerable to even low-power ultrasonic bath. The PDMS channel is exposed again by dipping the sample into the AZ300K developer as wet etcher for about 30 s (Step 7).

In Step 8, the exposed PDMS between the channel and the electrodes is bonded to a top cladding of PDMS after oxygen plasma treatment. The top cladding of PDMS is narrow enough to keep the outer part of electrodes exposed for electrical connection.
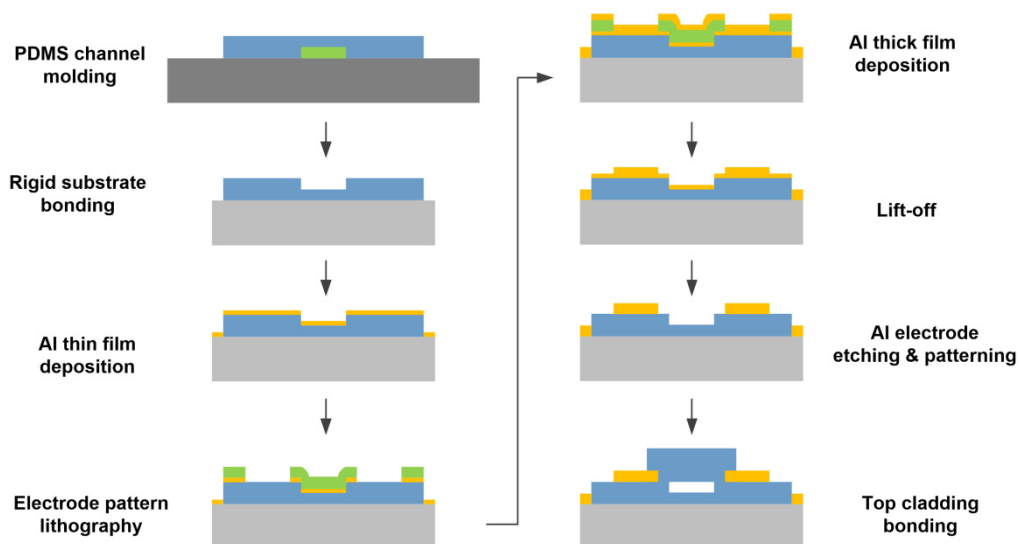

Fig. 2. Fabrication procedures of the polarization rotator. The dark grey color (Step 1) denotes silicon wafer, the green color represents AZ5214 photoresist, and the other colors follow the definitions in in Fig. 1(b) and 1(c).

The micrograph of fabricated device is shown in Fig. 3, focusing on the main part of PDMS channel and curvy aluminum electrodes. Since the bonding process for PDMS channel is performed manually, and the available time for bonding is less than 1 minute, it is

impossible to align the top PDMS cladding to meet the end of PDMS thin film. To get the smooth interfaces for light coupling and output observation, both ends of the bonded PDMS are cleaved. Before end-cleaving, DI water is filled into the channel and frozen, which provides a solid support to the soft PDMS channel wall. Otherwise, the PDMS channel would collapse during the cleavage. After the cleavage, the total length of waveguide (channel) is reduced to about 1 cm for each different sample, and the PR portion is much closer to the output port (about 1 mm) so that the influence of exit waveguide portion is alleviated. When the NLC of 5CB is applied to the end of PDMS channel, it flows in automatically due to the capillary effect. The temperature is maintained at about 25 °C to keep the nematic phase of NLC.
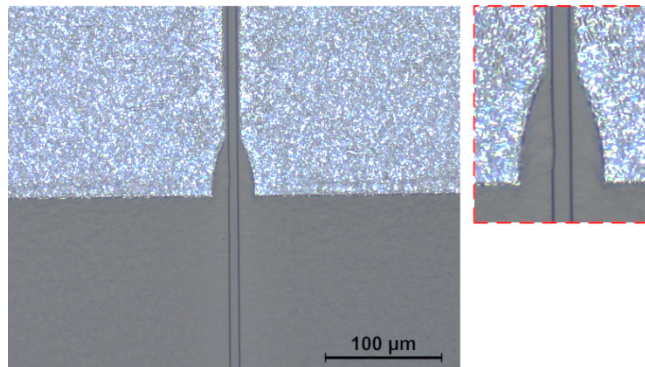

Fig. 3. Micrograph of the fabricated device (inset for clear view of the central part).

4. Experiments

There are mainly three parts in the test scheme (see Fig. 4), including the light coupling optics, the voltage driver and monitor, and also the end-view and top-view microscopes (not-shown in Fig. 4) for observation. The end-fire coupling is carried out using the coupling optics of a laser source (532 nm, output power 5 ~30 mW) with pigtail fiber, a polarization controller (Pol-controller) and a lens fiber (the nominal neck size of the focus spot is 2.5 ± 0.5 μm in diameter). The AC power supplier provides the driving voltage which is the sinusoidal wave at 1 kHz frequency and low DC bias (several mV). Two micro-probes are connected from the power supplier to the respective electrodes through micro-positioners. The top-view microscope is used for input coupling. The polarization rotation is indirectly observed by using a polarization filter (Pol-filter) inserted between the device output end and the end-view microscope. In this regard, the polarization rotation is transferred into the power modulation.
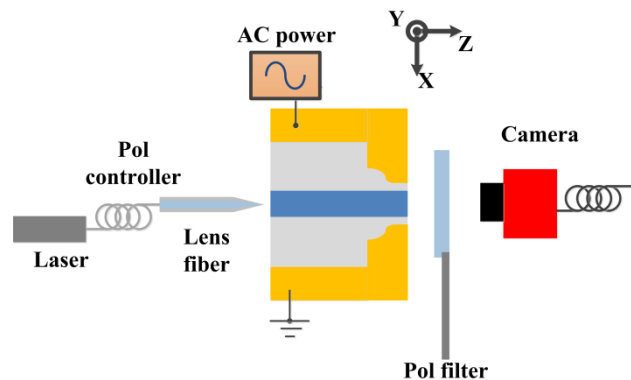

Fig. 4. Test setup for the proposed device in the end-fire scheme.

The main experiment results are shown in Fig. 5, with specific pass directions in Pol-filter, including the X (in parallel to the substrate plane) and Y directions (perpendicular with the substrate plane). Accordingly, the light propagates forward along the Z direction, with the fixed laser power of 10 mW. The results are recorded with the driving voltages (RMS) of 6.73 V (see Fig. 5(a)) and 40.63 V (see Fig. 5(b)) for the X-direction test, and also 6.73 V (see Fig. 5(c)) and 35.56 V (see Fig. 5(d)) for the Y-direction test, respectively. The measured X components of output power are plotted in Fig. 5(e). The sweeping range of the driving voltages is between about 6V and 50V, which keeps the NLC stabilized while avoiding breakdown from too strong electric field. It is seen that strong output (bright output spot) can be observed at low driving voltages (OFF-state), while weak output (dark output spot) is obtained at high driving voltages (ON-state). The opposite results are observed for the Y-direction test using the same driving voltages. The scattered light is mainly due to the relative shift between the PDMS waveguide and the electrodes in fabrication. In theory [9], the fabricated waveguide can support multi modes as for its relatively high refractive index (RI) contrast and large channel size, however, the fundamental mode achieves strongest excitation as shown in Fig. 5(a) and 5(d). The ON/OFF switching time is estimated to be less than 70 ms. Even faster switching can be achieved using a thinner channel [3].
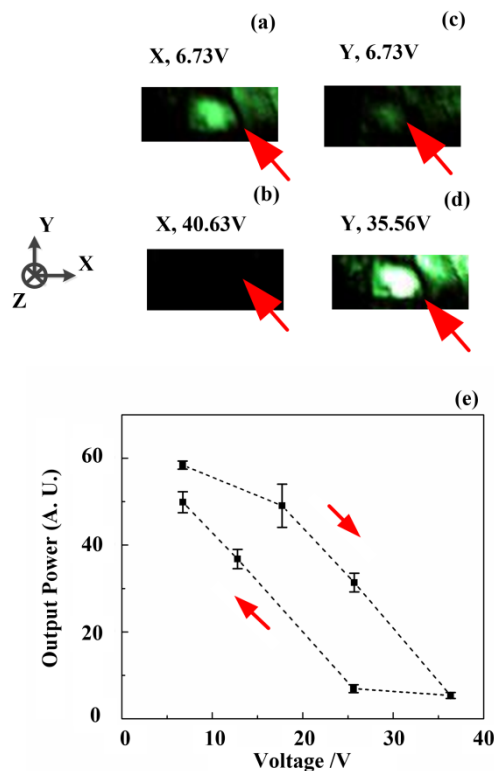

Fig. 5. (a) ~(d) Observed output spots to exemplify the switching of polarization at different driving voltages, and (e) output power versus driving voltage in the X-direction test, with the error bars indicating the confidence intervals.

The propagation loss in the waveguide is measured to be 9 dB/cm by capturing the top-view scattering light field, which is consistent with the previous reports [3,6,10] for the NLC-core waveguide at 532 nm. It is noted that a stronger laser power of about 15 mW is applied in the propagation loss measurement for better sensitivity. As for the coupling loss, it is mainly due to the mismatching between the PDMS waveguide and the focal spot from lens fiber, in which the channel is too thin to block some input light, and too wide to meet the

input mode field. The RI difference between NLC and air also contributes to the back reflection. As a rough estimation, the coupling loss is measured at the output end by comparing the light power (both polarizations at 6.73V) inside the channel to that over the whole plane, and it is found to be approximately 26 dB. It is noted the loss is underestimated since all the back scattering light and some of the side scattering light are excluded in the calculation. By considering the total loss budget, the light power reaches the working component of PR is approximately 0.004 mW, whose power density (about 0.25 $\mu W/\mu m^2$) is nearly three orders weaker than the typical value (0.16 $mW/\mu m^2$) in the nonlinear NLC devices e.g. nematicon [8]. It is thus confirmed that the polarization rotator works in the regime far from optical-field induced nonlinearity [8], and the NLC reorientation is exclusively due to the electric field.

With the above results, the electrically-switchable polarization rotation is thus confirmed experimentally.

As shown in Fig. 5(e), it is also seen that the response is not symmetric in the rise and fall paths, showing some hysteresis-like phenomenon. The hysteresis phenomena in pure or doped NLC, especially the first-order Freedericksz transition (FT), have been studied for decades [11–16], which can be useful for logical and bistable devices in optical data processing system [11,16]. The underlying mechanism generally involves two counteracting fields, such as optical and magnetic field [12], optical and low frequency electric field [13], magnetic field and electric field [14], surface anchoring and external driving field [15]. Different from the spatial soliton or nematicon [8], the first-order FT can be triggered under a relatively low light intensity (e.g. 200W/cm^2) [12,13]. Recently, the optical nonlinear case is reported, where coexistence of the diffracting and self-confined beam states is enabled by the optical FT [11]. The hysteresis effect can also be induced by optoelectronic feedback [16].

Without equipping optoelectronic feedback while staying away from optical nonlinear regime, the hysteresis-like phenomenon observed here is most related to the mechanism involving two counteracting fields. More specifically, the surface anchoring by homeotropic alignment (along the Y axis), and the driving electric field along the X axis, together contribute to the hysteresis-like phenomenon in the above experiments. In [15], it is pointed out that the first-order FT under external driving field can occur more easily when the NLC with $k = K_{11}/K_{33} < 1$ (e.g. 5CB here with $k = 0.83$ [12]) is applied using the homeotropic alignment. The symbols K_{11} and K_{33} denote the components of NLC elastic constant. Similarly, the influence of surface anchoring on first-order FT is experimentally revealed in [11], with the homogeneous alignment considered. It is noted that the hysteresis-like phenomenon here exhibits two continuous curves (resembles that in [12]), and is a bit different from the abrupt first-order FT loop. However, the underlying mechanism is expected to be similar.

Moreover, the relatively weak alignment effect from left/right PDMS side walls (see Fig. 1(b)) may impede the restoration of NLC direction when the driving electric field is lost, which also induce some extent of hysteresis during the switching process. The influence from optical light field can be neglected for the hysteresis-like phenomenon, since the driving electric field is about two orders higher than the optical electric field.

5. Conclusions

In conclusions, the polarization rotation is reported using the optofluidic planar NLC waveguide. In the device fabrication, the co-integration of PDMS and metal electrodes is solved by using a sacrificing Al thin layer. The electrically-switchable PR is confirmed in both orthogonal polarization directions (with respect to the substrate plane), and the hysteresis-like phenomenon is also observed during the switching. According to the numerical results in [3], the working wavelength of the planar NLC-PR can also be extended to the near infrared ones, e.g. 1550 nm. The planar NLC-PR design may be integrated into

NLC-based optical switches [3], flexible photonic devices [17], and optofluidic photonic integrated circuits [10].

References

1. I. C. Khoo, *Liquid Crystals* (Hoboken, N.J.: Wiley-Interscience, 2007).
2. A. K. Pitilakis, D. C. Zografopoulos, and E. E. Kriezis, "In-line polarization controller based on liquid-crystal photonic crystal fibers," J. Lightwave Technol. **29**(17), 2560–2569 (2011).
3. T. Li, Q. Chen, W. Yu, and X. Zhang, "Planar polarization-routing optical cross-connects using nematic liquid crystal waveguides," Opt. Express **26**(1), 402–418 (2018).
4. S. Strunck, A. Gaebler, O. H. Karabey, M. Jost, and R. Jakoby, "Electrically reconfigurable waveguide polarizer using liquid crystal technology for Ka-band applications," in 2014 44th European Microwave Conference, 2014, pp. 508–511.
5. Q. Xu, L. Chen, M. G. Wood, P. Sun, and R. M. Reano, "Electrically tunable optical polarization rotation on a silicon chip using Berry's phase," Nat. Commun. **5**(1), 5337 (2014).
6. A. Alessandro, S. Member, L. Martini, G. Gilardi, R. Beccherelli, and R. Asquini, "Polarization-independent nematic liquid crystal waveguides for optofluidic applications," IEEE Photonics Technol. Lett. **27**(16), 1709–1712 (2015).
7. P. Fiala, C. Dorrer, and K. Marshall, "Twisted-nematic liquid crystal polarization rotators for broadband laser applications," in CLEO: 2015, OSA Technical Digest (online) (Optical Society of America, 2015), paper JW2A.68.
8. G. Assanto, A. Fratalocchi, and M. Peccianti, "Spatial solitons in nematic liquid crystals: from bulk to discrete," Opt. Express **15**(8), 5248–5259 (2007).
9. K. Okamoto, *Fundamentals of Optical Waveguides* (New York, NY, USA: Academic, 2006).
10. D. C. Zografopoulos, R. Asquini, E. E. Kriezis, A. d'Alessandro, and R. Beccherelli, "Guided-wave liquid-crystal photonics," Lab Chip **12**(19), 3598–3610 (2012).
11. A. Piccardi, A. Alberucci, N. Kravets, G. Assanto, O. Buchnev, and M. Kaczmarek, "Light beam hysteresis in liquid crystals," 2014 Fotonica AEIT Italian Conference on Photonics Technologies, 2014, pp. 1–3.
12. A. J. Karn, S. M. Arakelian, Y. R. Shen, and H. L. Ong, "Observation of magnetic-field-induced first-order optical Fréedericksz transition in a nematic film," Phys. Rev. Lett. **57**(4), 448–451 (1986).
13. S.-H. Chen and J. J. Wu, "Observation of first-order Freedericksz transition in a nematic film induced by electric and optical fields," Appl. Phys. Lett. **52**(23), 1998–2000 (1988).
14. B. J. Frisken and P. Palffy-Muhoray, "Freedericksz transitions in nematic liquid crystals: The effects of an in-plane electric field," Phys. Rev. A Gen. Phys. **40**(10), 6099–6102 (1989).
15. G. Yang, J. Shi, and Y. Liang, "Surface anchoring energy and the first order Fréedericksz transition of a NLC cell," Liq. Cryst. **27**(7), 875–882 (2000).
16. E.Melnikova, A.Tolstik, "Realization of logical operations, bistability and self-oscillations on the basis of optoelectronic liquid-crystal elements using S-effect," Proc. SPIE **3318**, 515–518 (1998,).
17. J. Hu, L. Li, H. Lin, P. Zhang, W. Zhou, and Z. Ma, "Flexible integrated photonics: where materials, mechanics and optics meet," Opt. Mater. Express **3**(9), 1313–1331 (2013).